IEICE TRANS. ELECTRON., VOL.E96–C, NO.5 MAY 2013

PAPER

Accurate Permittivity Estimation Method with Iterative Waveform Correction for UWB Internal Imaging Radar

Ryunosuke SOUMA[†a)], ***Student Member***, **Shouhei KIDERA**[†], ***and*** **Tetsuo KIRIMOTO**[†], ***Members***

SUMMARY Ultra-wideband (UWB) pulse radar has high range resolution and permeability in a dielectric medium, and has great potential for the non-destructive inspection or early-stage detection of breast cancer. As an accurate and high-resolution imaging method for targets embedded in a dielectric medium, extended range points migration (RPM) has been developed. Although this method offers an accurate internal target image in a homogeneous media, it assumes the permittivity of the dielectric medium is given, which is not practical for general applications. Although there are various permittivity estimation methods, they have essential problems that are not suitable for clear, dielectric boundaries like walls, or is not applicable to an unknown and arbitrary shape of dielectric medium. To overcome the above drawbacks, we newly propose a permittivity estimation method suitable for various shapes of dielectric media with a clear boundary, where the dielectric boundary points and their normal vectors are accurately determined by the original RPM method. In addition, our method iteratively compensates for the scattered waveform deformation using a finite-difference time domain (FDTD) method to enhance the accuracy of the permittivity estimation. Results from a numerical simulation demonstrate that our method achieves accurate permittivity estimation even for a dielectric medium of wavelength size.

key words: *UWB pulse radar, permittivity estimation, internal imaging, non-parametric approach, range points migration*

1. Introduction

Ultra-wideband (UWB) signals were approved for commercial use by the Federal Communications Commission (FCC) in 2002, and have a frequency width of over 500 MHz or a 10-dB fractional bandwidth of over 25% [1]. Since a radar system employing a UWB signal has high range resolution and desirable dielectric penetrating ability, it is promising for a wide variety of internal imaging applications. For instance, the system can be non-destructively used to determine the location and shape of a rebar or pipe, to detect cavities or cracks within walls [2], or in medicine to detect breast tumors at an early stage [3]. Various internal imaging techniques, such as the time-reversal method [4] and the space-time beamforming method [3], have been established for these applications. However, these algorithms are based on signal waveform integrations, which often require a large computational calculation or have insufficient accuracy to identify the detailed structure of targets.

To overcome the above problem, we have already proposed a fast and accurate UWB imaging method for targets buried in a dielectric medium [5]. This method is based on the advanced principle of the range points migration (RPM) method [6], which accurately determines the propagation path in a dielectric medium by exploiting the target boundary points and their normal vectors under a geometrical optics approximation. Although this method enhances an imaging accuracy and remarkably reduces the computational amount by specifying boundary extraction, it is based on the assumption that the permittivity of the dielectric medium is preliminarily given. This assumption is often invalid for actual internal sensing scenes, such as non-destructive inspection for an unknown medium.

As a solution to this issue, there are various types of permittivity estimation methods that are based on numerical solutions of domain integral equations [7], [8] or that employ time delays and known dielectric structures based on the geometric optics approximation for through-the-wall applications [9]–[11]. Although the former method [7] or [8] can treat inhomogeneous dielectric media, its accuracy or spatial resolution strongly depends on the assumed pixel size (directly related to the number of optimization variables. Also, there is a severe limitation of space discretization size to avoid sluggish convergence in multi-dimensional optimizations. In contrast, the method in [9]–[11] requires relatively smaller computational resources compared with methods like [7] and [8]. However, implementation of the method assumes a known and simple shape for dielectric medium, such as a rectangle.

To ensure the permittivity estimation is suitable for the internal imaging assumed in [6], this paper proposes an accurate method of permittivity estimation exploiting features of the RPM method. In particular, this method employs the dielectric boundary location and its normal vector correctly produced by the original RPM method [6]. The actual time delay in propagating through the dielectric medium can then be accurately estimated from the recorded transmissive data. Moreover, in the case of a dielectric medium with a wavelength scale, the transmissive waveform differs from the transmitted waveform, and it reduces the accuracy of the measurement of the time delay. Then, the proposed method has the additional property of compensating for the error caused by the above waveform deformation by iteratively generating the observation data using a finite-difference time domain (FDTD) method. The numerical-simulation-based validations show that our method achieves accurate permittivity estimation, by taking a completely non-parametric approach even for targets of a wavelength scale.

Manuscript received July 31, 2012.
Manuscript revised November 1, 2012.

[†]The authors are with the Graduate School of Informatics and Engineering, The University of Electro-Communications, Chofu-shi, 182-8585 Japan.
a) E-mail: souma@secure.ee.uec.ac.jp

DOI: 10.1587/transele.E96.C.730

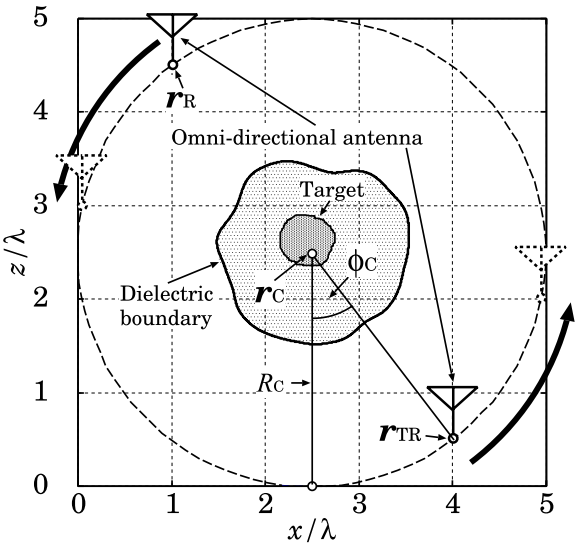

Fig. 1 System model.

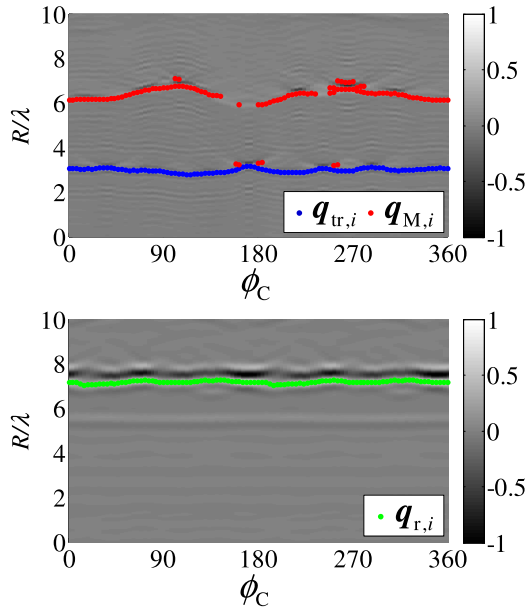

Fig. 2 Outputs of Wiener filter $S_{TR}(\boldsymbol{r}_{TR}, R)$ (upper) and $S_R(\boldsymbol{r}_R, R)$ (lower), and extracted range points.

2. System Model

Figure 1 shows the system model. It assumes that a target and homogeneous dielectric medium have an arbitrary shape with a clear boundary. The internal target can be located anywhere within the dielectric medium, which also has arbitrary position. A mono-cycle pulse is used as the transmitting signal, the center wavelength of which is defines as λ. The propagation speed c of the radio wave in air is a known constant. Two omni-directional antennas scan along the circle with a center $\boldsymbol{r}_c$ and radius R_c that completely surrounds a dielectric object as shown in Fig. 1. One transmitting and receiving antenna is located at $\boldsymbol{r}_{TR} = (X_{tr}, Z_{tr})$, and an antenna playing only a receiving role is located at $\boldsymbol{r}_R = (X_r, Z_r)$, where $\boldsymbol{r}_c = (\boldsymbol{r}_{TR} + \boldsymbol{r}_R)/2$ holds. $S_{TR}(\boldsymbol{r}_{TR}, R)$ and $S_R(\boldsymbol{r}_R, R)$ are defined as the outputs of the Wiener filter at antenna positions $\boldsymbol{r}_{TR}$ and $\boldsymbol{r}_R$, respectively, where $R = ct/2$ is expressed by time t (see Ref. [6] for details). Figure 2 illustrates the examples of $S_{TR}(\boldsymbol{r}_{TR}, R)$ and $S_R(\boldsymbol{r}_R, R)$, where the target and dielectric medium are assumed as in Fig. 1.

3. Conventional Method

Various types of permittivity estimation methods have been developed in applications to non-destructive measurement analysis or non-invasive medical imaging, such as breast cancer detection using UWB radar. Because a direct comparison of these conventional methods or the proposed approach would be a mismatch as each method deals with different types of parameters, this section focuses on only the general advantages and disadvantages of each conventional method when referring to a feature of the proposed method. One typical method is based on the numerical solution of the domain integral equation [7], [8] for inhomogeneous dielectric medium, and the other popular approach exploits the transmissive time delay for rectangular or cuboid dielectric structures for through-the-wall imaging [9]–[11]. Despite furnishing permittivity or conductivity estimates for inhomogeneous dielectric media, the method used in [7] or [8] requires space discretization in solving the domain integral equations, and its reconstruction accuracy or resolution crucially depends on the assumed pixel size. Thus, if we try to enhance the reconstruction accuracy or resolution the method requires enormous calculation overheads because of the large dimensional arrays from space analysis that generally hinder convergence rates in multi-dimensional optimizations.

In contrast, the method of [9], [10] or [11] estimates the wall's dielectric property by employing the observed time delay and a known wall structure, based on the geometrical optics approximation. Whereas the computational cost of this type of method is relatively small compared with methods like [7] and [8], it requires an assumption that the dielectric medium has a simple structure, either rectangular or cuboid, and its shape is completely known. In addition, they do not assume that the dielectric medium includes an object with different dielectric properties, as assumed in this study. According to the above discussions, these conventional approaches are not completely suitable to the current problem, namely, an unknown clear boundary for the dielectric medium and internal objects.

4. Proposed Method

To overcome the above difficulties, this paper proposes a novel non-parametric permittivity estimation method that is suitable for an clear dielectric boundary. The methodology of this method is detailed as follows.

4.1 Dielectric Boundary Extraction with RPM

First, this method employs the dielectric boundary points produced by the original RPM method, which achieves extremely accurate imaging employing the extracted range points defined as $\boldsymbol{q}_{\mathrm{tr},i} = (X_{\mathrm{tr},i}, Z_{\mathrm{tr},i}, R_{\mathrm{tr},i}), (i = 1, ..., N_{\mathrm{tr}})$. These components are extracted from the local maxima $S_{\mathrm{TR}}(\boldsymbol{r}_{\mathrm{TR}}, R)$, and N_{tr} denotes the total number of the range points as shown in Fig. 2. The RPM method then directly converts these range points to the target boundary points as $\boldsymbol{r}_i = (x_i, z_i), (i = 1, ..., N_{\mathrm{tr}})$, where one-to-one correspondence is satisfied [6]. Furthermore, in order to avoid a sparse distribution of these points, the Envelope interpolation scheme is adopted as similar in [12]. A set of these target points is defined as $\mathcal{T}_{\mathrm{rpm}}$. Note that the normal vector at each target boundary point is calculated without a derivative operation as $\boldsymbol{e}_{\mathrm{n},i} = (X_{\mathrm{tr},i} - x_i, Z_{\mathrm{tr},i} - z_i)/R_{\mathrm{tr},i}$.

4.2 Permittivity Estimation with Transmissive Data

For calculating the propagation path, the incident and exit points $(\hat{\boldsymbol{r}}_{\mathrm{I}}(\epsilon_{\mathrm{t}}), \hat{\boldsymbol{r}}_{\mathrm{E}}(\epsilon_{\mathrm{t}}))$ on the dielectric boundary are determined by the Snell's law:

$$(\hat{\boldsymbol{r}}_{\mathrm{I}}(\epsilon_{\mathrm{t}}), \hat{\boldsymbol{r}}_{\mathrm{E}}(\epsilon_{\mathrm{t}})) = \underset{(\boldsymbol{r}_i, \boldsymbol{r}_j) \in \mathcal{T}_{\mathrm{rpm}}^2}{\arg\min} \left\{ \left\| \boldsymbol{e}_i(\epsilon_{\mathrm{t}}) - \boldsymbol{e}_{i,j} \right\|^2 + \left\| \boldsymbol{e}_j(\epsilon_{\mathrm{t}}) - \boldsymbol{e}_{i,j} \right\|^2 \right\}, \quad (1)$$

where ϵ_{t} is a relative permittivity of dielectric medium, $\boldsymbol{e}_i(\epsilon_{\mathrm{t}}) = \boldsymbol{R}_o\left(\theta_i(\epsilon_{\mathrm{t}})\right)\left(-\boldsymbol{e}_{\mathrm{n},i}\right)$, $\boldsymbol{e}_j(\epsilon_{\mathrm{t}}) = \boldsymbol{R}_o\left(\theta_j(\epsilon_{\mathrm{t}})\right)\left(-\boldsymbol{e}_{\mathrm{n},j}\right)$ and $\boldsymbol{e}_{i,j} = \left(\boldsymbol{r}_i - \boldsymbol{r}_j\right) / \left\| \boldsymbol{r}_i - \boldsymbol{r}_j \right\|$. $\boldsymbol{R}_o(\theta)$ is a rotation matrix in the counterclockwise direction, and $\theta_i(\epsilon_{\mathrm{t}})$ and $\theta_j(\epsilon_{\mathrm{t}})$ denote the refraction angles calculated by Snell's law. Figure 3 shows the estimated dielectric boundary produced by Envelope, and spatial relationship among the incident, exit boundary points and the antenna locations. Next, the propagation distance from $\boldsymbol{r}_{\mathrm{TR},i}$ to $\boldsymbol{r}_{\mathrm{R},i}$ is calculated:

$$R(\epsilon_{\mathrm{t}}; X_{\mathrm{r},i}, Z_{\mathrm{r},i}) = \frac{1}{2}\Big\{ \left\| \hat{\boldsymbol{r}}_{\mathrm{I}}(\epsilon_{\mathrm{t}}) - \boldsymbol{r}_{\mathrm{TR},i} \right\| + \sqrt{\epsilon_{\mathrm{t}}} \left\| \hat{\boldsymbol{r}}_{\mathrm{I}}(\epsilon_{\mathrm{t}}) - \hat{\boldsymbol{r}}_{\mathrm{E}}(\epsilon_{\mathrm{t}}) \right\| + \left\| \hat{\boldsymbol{r}}_{\mathrm{E}}(\epsilon_{\mathrm{t}}) - \boldsymbol{r}_{\mathrm{R},i} \right\| \Big\}. \quad (2)$$

The relative permittivity for each range point is then determined by

$$\epsilon_{\mathrm{t}}^{\mathrm{init}}\left(\boldsymbol{q}_{\mathrm{r},i}\right) = \underset{\epsilon_{\mathrm{t}}}{\arg\min} \left| R(\epsilon_{\mathrm{t}} : X_{\mathrm{r},i}, Z_{\mathrm{r},i}) - R_{\mathrm{r},i} \right|, \quad (3)$$

where $\boldsymbol{q}_{\mathrm{r},i} = (X_{\mathrm{r},i}, Z_{\mathrm{r},i}, R_{\mathrm{r},i}), (i = 1, ..., N_{\mathrm{r}})$ are extracted from the maxima of $S_{\mathrm{R}}(X, Z, R)$ as shown in Fig. 2. Using all the transmissive range points, the initial relative permittivity $\hat{\epsilon}_{\mathrm{t}}^{\mathrm{init}}$ is estimated as

$$\hat{\epsilon}_{\mathrm{t}}^{\mathrm{init}} = \frac{\sum_{\boldsymbol{q}_{\mathrm{r},i} \in Q} S_{\mathrm{R}}\left(\boldsymbol{q}_{\mathrm{r},i}\right) \epsilon_{\mathrm{t}}^{\mathrm{init}}\left(\boldsymbol{q}_{\mathrm{r},i}\right)}{\sum_{\boldsymbol{q}_{\mathrm{r},i} \in Q} S_{\mathrm{R}}\left(\boldsymbol{q}_{\mathrm{r},i}\right)}, \quad (4)$$

where $Q = \left\{ \boldsymbol{q}_{\mathrm{r},i} \middle| \left| \epsilon_{\mathrm{t}}^{\mathrm{init}}\left(\boldsymbol{q}_{\mathrm{r},i}\right) - \bar{\epsilon}_{\mathrm{t}}^{\mathrm{init}} \right| < \Delta\epsilon_{\mathrm{t}}^{\mathrm{init}} \right\}$, and $\bar{\epsilon}_{\mathrm{t}}^{\mathrm{init}}$ is the mode value calculated from the distribution of $\epsilon_{\mathrm{t}}^{\mathrm{init}}\left(\boldsymbol{q}_{\mathrm{r},i}\right)$, $\Delta\epsilon_{\mathrm{t}}^{\mathrm{init}}$ is the threshold to eliminate outliers.

Note that the above procedure is basically derived from the geometrical optics approximation, where the frequency characteristic in transmissive phenomena is not taken into consideration. However, in the case of a dielectric medium of wavelength scale, this frequency characteristic is not negligible and it causes the waveform deformation of transmissive data, which reduces the accuracy of the relative permittivity estimation, owing to the inaccuracy of the range points. The upper and lower sides of Fig. 4 show the examples of transmitted and transmissive waveforms where the phases of both waveforms are compensated by their actual time delays.

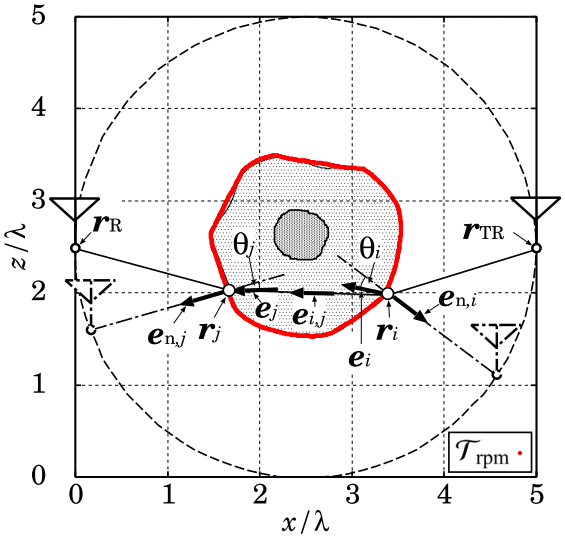

Fig. 3 Spatial relationship among the incident, exit boundary points and antenna locations, and obtained dielectric boundary points as $\mathcal{T}_{\mathrm{rpm}}$.

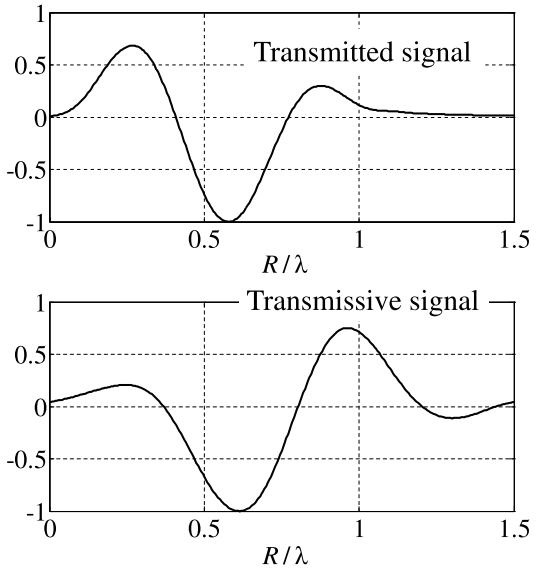

Fig. 4 Transmitted (upper) and transmissive signal waveforms (lower).

4.3 Waveform Correction with FDTD Method

To mitigate this type of accuracy degradation, we introduce an iterative procedure to compensate the range point error caused by waveform deformation using an FDTD. Specifically, we regenerate the transmissive data as $\tilde{S}_{\mathrm{R}}(\boldsymbol{r}_{\mathrm{R}}, R)$ using the FDTD, where the dielectric boundary points as $\mathcal{T}_{\mathrm{rpm}}$ and the estimated relative permittivity as $\hat{\epsilon}_{\mathrm{t}}^{\mathrm{init}}$ are employed for FDTD data generation. Next, the range correction $\Delta R\left(\boldsymbol{q}_{\mathrm{r},i}\right)$ at each range point $\boldsymbol{q}_{\mathrm{r},i}$ is determined from the peak shift of the correlation function between the measured $S_{\mathrm{R}}(\boldsymbol{r}_{\mathrm{R}}, R)$ and the regenerated transmissive data $\tilde{S}_{\mathrm{R}}(\boldsymbol{r}_{\mathrm{R}}, R)$. The estimated relative permittivity $\epsilon_{\mathrm{t}}\left(\boldsymbol{q}_{\mathrm{r},i}\right)$ for each range point is then corrected:

$$\epsilon_{\mathrm{t}}\left(\boldsymbol{q}_{\mathrm{r},i}\right) = \left\{ \sqrt{\hat{\epsilon}_{\mathrm{t}}^{\mathrm{init}}} + \frac{\Delta R\left(\boldsymbol{q}_{\mathrm{r},i}\right)}{L_{\epsilon}\left(\boldsymbol{q}_{\mathrm{r},i}\right)} \right\}^{2}, \tag{5}$$

where $L_{\epsilon}\left(\boldsymbol{q}_{\mathrm{r},i}\right) = \sqrt{\hat{\epsilon}_{\mathrm{t}}^{\mathrm{init}}}\left\|\hat{\boldsymbol{r}}_{\mathrm{I}}(\epsilon_{\mathrm{t}}) - \hat{\boldsymbol{r}}_{\mathrm{E}}(\epsilon_{\mathrm{t}})\right\|$ is the estimated propagation distance in the dielectric medium for $\boldsymbol{q}_{\mathrm{r},i}$, which is previously determined by Eq. (2). Finally, the relative permittivity $\hat{\epsilon}_{\mathrm{t}}$ is updated as

$$\hat{\epsilon}_{\mathrm{t}} = \frac{\sum_{\boldsymbol{q}_{\mathrm{r},i}\in\tilde{Q}} S_{\mathrm{R}}\left(\boldsymbol{q}_{\mathrm{r},i}\right)\epsilon_{\mathrm{t}}\left(\boldsymbol{q}_{\mathrm{r},i}\right)}{\sum_{\boldsymbol{q}_{\mathrm{r},i}\in\tilde{Q}} S_{\mathrm{R}}\left(\boldsymbol{q}_{\mathrm{r},i}\right)}, \tag{6}$$

where $\tilde{Q} = \left\{\boldsymbol{q}_{r,i} \middle| \left|\epsilon_{\mathrm{t}}\left(\boldsymbol{q}_{r,i}\right) - \bar{\epsilon}_{\mathrm{t}}\right| < \Delta\tilde{\epsilon}_{\mathrm{t}}\right\}$ and $\bar{\epsilon}_{\mathrm{t}}$ is the mode value calculated from the distribution of $\epsilon_{\mathrm{t}}\left(\boldsymbol{q}_{\mathrm{r},i}\right)$, $\Delta\tilde{\epsilon}_{\mathrm{t}}$ is a threshold to eliminate outliers. The above process is repeated until the difference between the updated value and previously estimated value is less than the threshold $\Delta\tilde{\epsilon}_{\mathrm{t}}$.

4.4 Procedure of Proposed Method

The actual procedure of this method is summarized as follows.

Step 1) Dielectric boundary points are obtained by RPM, where the sparse area is interpolated by Envelope method. A set of these points as $\mathcal{T}_{\mathrm{rpm}}$ is created.

Step 2) Using all transmissive range points $\boldsymbol{q}_{\mathrm{r},i}$, the initial relative permittivity $\hat{\epsilon}_{\mathrm{t}}^{\mathrm{init}}$ is estimated by Eqs. (3) and (4), where the propagation distance for each range point is determined by Eq. (2). Additionally, $\hat{\epsilon}_{\mathrm{t}}^{\mathrm{b}} = \hat{\epsilon}_{\mathrm{t}}^{\mathrm{init}}$ is set.

Step 3) Transmissive data are regenerated as $\tilde{S}_{\mathrm{R}}(\boldsymbol{r}_{\mathrm{R}}, R)$ using the FDTD, where the estimated dielectric boundary $\mathcal{T}_{\mathrm{rpm}}$ and the previously estimated relative permittivity $\hat{\epsilon}_{\mathrm{t}}^{\mathrm{b}}$ are employed.

Step 4) The relative permittivity is updated as $\hat{\epsilon}_{\mathrm{t}}$ by assessing the peak shift of the correlation function between $\tilde{S}_{\mathrm{R}}(\boldsymbol{r}_{\mathrm{R}}, R)$ and $S_{\mathrm{R}}(\boldsymbol{r}_{\mathrm{R}}, R)$ in Eqs. (5) and (6).

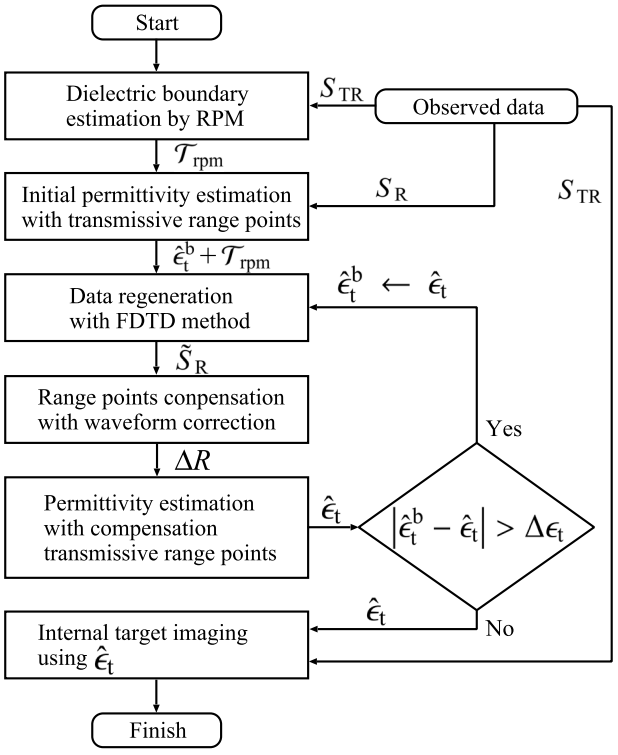

Fig. 5 Flowchart of the proposed method.

Step 5) If the following condition is satisfied,

$$\left|\hat{\epsilon}_{\mathrm{t}}^{\mathrm{b}} - \hat{\epsilon}_{\mathrm{t}}\right| > \Delta\epsilon_{\mathrm{t}}, \tag{7}$$

$\hat{\epsilon}_{\mathrm{t}}^{\mathrm{b}} \leftarrow \hat{\epsilon}_{\mathrm{t}}$ is set and return to the Step 3), where $\Delta\epsilon_{\mathrm{t}}$ is the threshold. Otherwise, move on to Step 6).

Step 6) The internal target boundary is produced using range points $\boldsymbol{q}_{\mathrm{M},i}$ and $\hat{\epsilon}_{\mathrm{t}}$ by the method described in [5], where $\boldsymbol{q}_{\mathrm{M},i}$ expresses the range points extracted from the local maxima $S_{\mathrm{TR}}(\boldsymbol{r}_{\mathrm{TR}}, R)$ as shown in Fig. 2.

Figure 5 shows the flowchart of the proposed method. A notable advantage of the proposed method is that it can deal with an arbitrary dielectric boundary, and the accuracy of the internal image can be enhanced using the correct relative permittivity obtained by compensating for the frequency characteristic of the transmissive wave.

5. Performance Evaluation in Numerical Simulation

This section presents the performance validation of the proposed method, where the observation data are created by employing the FDTD method. Here, to assess the versatility of our method, two types of boundary shape for the target and dielectric medium are assumed, labeled case (a) and case (b) in Fig. 6. Here, the shape of the dielectric boundary in case (b) is generated by giving white Gaussian values along the radial direction from the origin $(2.5\lambda, 2.5\lambda)$ with mean value 1λ and standard deviation 2λ. Then, these fluctuations are spatially smoothed using a Gaussian function

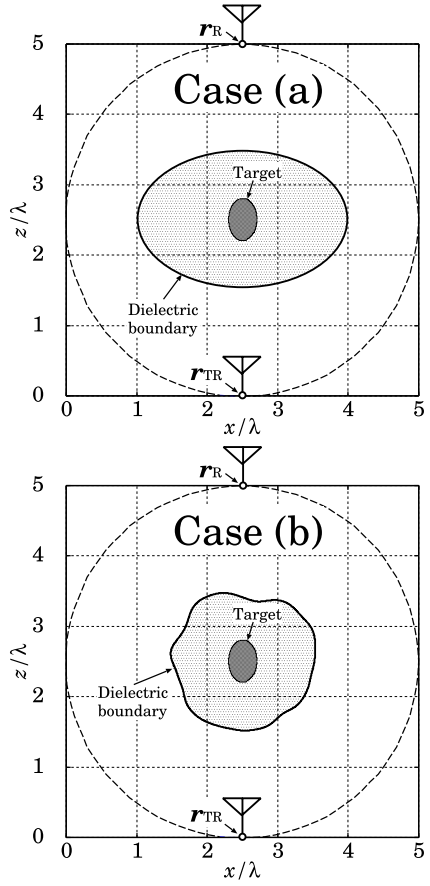

Fig. 6 Assumed dielectric media and internal targets (upper:case (a), lower:case (b)).

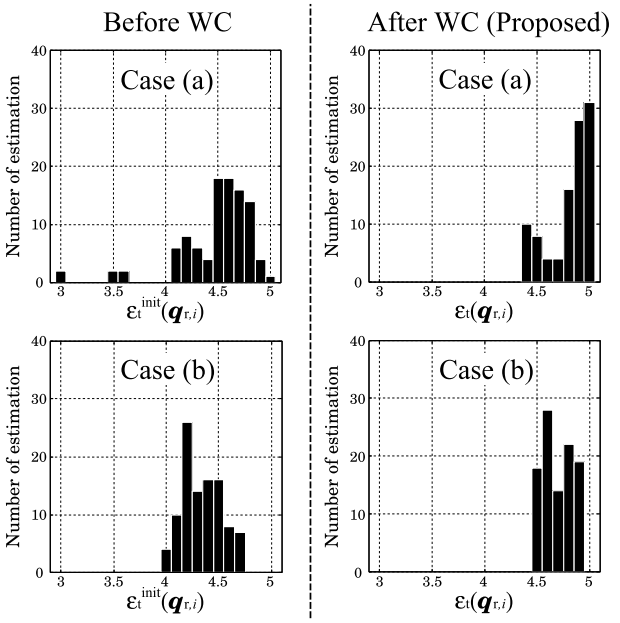

Fig. 7 Histograms of estimated relative permittivity before (left) and after (right) WC (proposed method) in noiseless situation (upper:case (a), lower:case (b)).

with correlation length is 0.3λ. In both cases, the conductivity of the target is set to 1.0×10^7 S/m, and the conductivity and relative permittivity of the dielectric medium are set to 0.01 S/m and $\epsilon_t = 5.0$. A noiseless situation is assumed. $\boldsymbol{r}_c = (2.5\lambda, 2.5\lambda)$ and $R_c = 2.5\lambda$ are set, and the scanning sample of the antenna is 101 uniformly spaced points. $\Delta\epsilon_t^{init} = \Delta\tilde{\epsilon}_t = 0.5$, and $\Delta\epsilon_t = 0.1$ are set in the proposed method. In the FDTD simulation, the induced current waveform at the transmitting antenna is defined as

$$i(t) = \begin{cases} (1 - \cos(2\pi t/T))\sin(2\pi t/T), & (0 < t \le T) \\ 0, \ (\text{otherwise}), \end{cases} \tag{8}$$

where $T = \lambda/c$. The time step interval for the FDTD calculation is set to $T/200$, and each spatial cell size along the x and z axes is $\lambda/80$.

Figure 7 presents histograms of the estimated relative permittivity obtained at each range point before and after (left and right panels resp.) waveform compensation (WC), namely $\epsilon_t^{init}\left(\boldsymbol{q}_{r,i}\right)$ in Eq. (3), and $\epsilon_t\left(\boldsymbol{q}_{r,i}\right)$ in Eq. (5) for each dielectric medium case. As shown for these figures, the mean and standard deviation of the estimated relative permittivity in both cases are considerably improved by the waveform correction in Eq. (5) in each case. The estimated relative permittivities before and after WC are $\hat{\epsilon}_t^{init} = 4.66$ (relative error: 6.8%) and $\hat{\epsilon}_t = 4.91$ (relative error: 1.8%) in the case (a), and $\hat{\epsilon}_t^{init} = 4.39$ (relative error: 12.2%) and $\hat{\epsilon}_t = 4.70$ (relative error: 6.0%) in the case (b). The number of WC iterations is four in case (a), and three in case (b). These results demonstrate that the waveform correction approach is considerably effective regardless of the dielectric shapes. Here, we confirm that each estimation of the relative permittivity has a smaller bias from the actual relative permittivity regardless whether WC is used or not. The reason for this bias is that a received signal at $\boldsymbol{r}_R$ includes a small component of a creeping wave propagating along the dielectric medium boundary, that causes a near-side range estimation, namely, incurring smaller assessment of the relative permittivity. Figure 8 shows the internal target boundary points estimated by the method described in [5] before and after WC (left and right panels resp.) for each case. These results also show that the internal estimation images are correctly shifted to the actual boundary by the relative permittivity compensation. In addition, the image comparison between the cases (a) and (b), clarifies that our proposed method is hard to be affected by the dielectric shape, and this is one of the most important advantage over method in the literature [9,10,11]. Note that, due to the round-off error in discretizing the dielectric medium or the internal target shapes for an FDTD calculation, there is a slight asymmetry in the internal image obtained in case (a) in Fig. 8, regardless of the symmetrical observation geometry. It should be also noted that there is an invisible area in both target boundaries because the range points from this shadow area are not retrieved, owing to a distorted propagation path depending on the shape of the dielectric boundary. Shadowing is a cru-

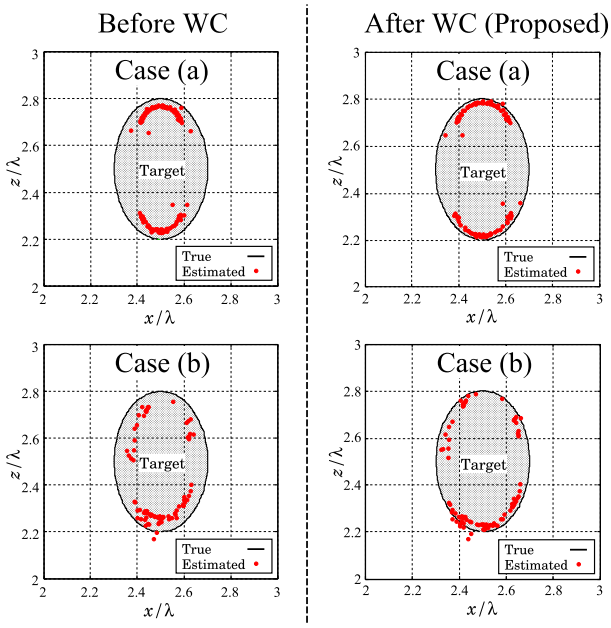

Fig. 8 Estimeted internal image in noiseless situation (left: before WC, right: after WC (proposed method)) (upper:case (a), lower:case (b)).

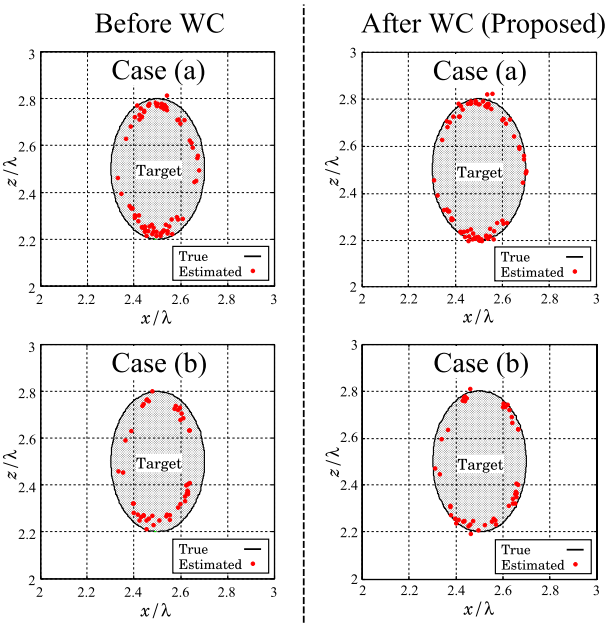

Fig. 9 Estimated internal image at S/N = 20 dB (left: before WC, right: after WC) (upper:case (a), lower:case (b)).

cial problem in the original internal imaging method [5], but is an independent issue in the proposed permittivity estimation method. One promising solution to this problem is the method proposed in [13], where the multi-static observation model is introduced. Furthermore, the computation time of the permittivity estimation is around 6 hours with a Xeon 3.0 GHz processor, including the time required for two cycle of FDTD data regeneration.

Next, the noisy signals are considered. White Gaussian noise is added to $S_{\mathrm{TR}}(X,Z,R)$ and $S_{\mathrm{R}}(X,Z,R)$, where the signal-to-noise ratio (S/N) is defined as the ratio of the peak instantaneous signal power to the average noise power after applying the matched filter. With S/N = 20 dB, $\hat{\epsilon}_{\mathrm{t}}^{\mathrm{init}} = 4.71$ (relative error: 5.8%) and $\hat{\epsilon}_{\mathrm{t}} = 4.86$ (relative error: 2.8%) in the case (a), and $\hat{\epsilon}_{\mathrm{t}}^{\mathrm{init}} = 4.45$ (relative error: 11.0%) and $\hat{\epsilon}_{\mathrm{t}} = 4.72$ (relative error: 5.6%) in the case (b). The number of WC iterations is three in both cases. Figure 9 shows the same view as in Fig. 8 for S/N = 20 dB. This result also verifies that the proposed method accomplishes robust and accurate internal imaging using an accurately estimated permittivity even with noisy signals.

Finally, for a quantitative analysis, an evaluation criterion for image accuracy is introduced as

$$e_{\mathrm{r}}\left(\boldsymbol{q}_{\mathrm{M},i}\right) = \min_{\boldsymbol{r}_{\mathrm{true}}} \left\| \boldsymbol{r}_{\mathrm{M}}\left(\boldsymbol{q}_{\mathrm{M},i}\right) - \boldsymbol{r}_{\mathrm{true}} \right\|, \tag{9}$$

where $\boldsymbol{r}_{\mathrm{true}}$ is the location of the true target points, and $\boldsymbol{r}_{\mathrm{M}}\left(\boldsymbol{q}_{\mathrm{M},i}\right)$ determines the estimated internal target points created by the method described in [5]. For case (a) and case (b) respectively, Fig. 10 shows the number of estimated target points for each $e_{\mathrm{r}}\left(\boldsymbol{q}_{\mathrm{M},i}\right)$ in the noiseless case and for S/N = 20 dB, before and after WC. This figure quantitatively demonstrates that the accuracy of target points is considerably enhanced even in the noisy case owing to the effect of range point compensation with FDTD data regeneration, in both cases. Note that, the number of the estimated target points in case (b) is relatively smaller than that in case (a). This is because in the case (b), the dielectric medium boundary has some concave region, and this causes difficulty for

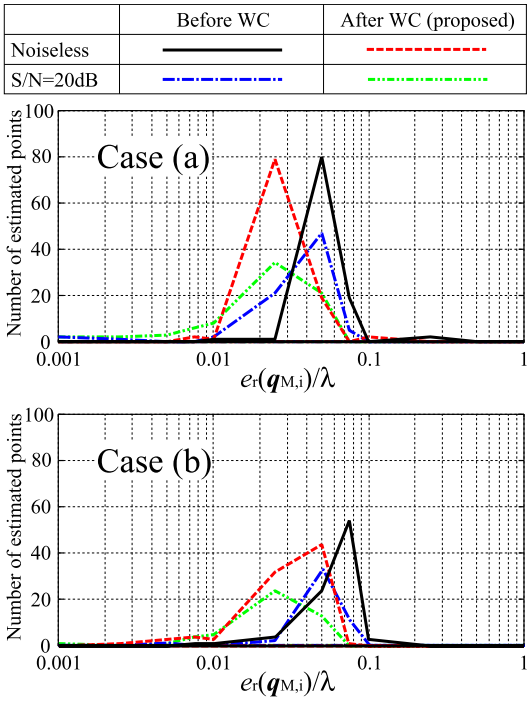

Fig. 10 Number of estimated points before and after range points compensation in each $e_{\mathrm{r}}\left(\boldsymbol{q}_{\mathrm{M},i}\right)$ at noiseless and S/N = 20 dB situation (upper:case (a), lower:case (b)).

Table 1 Value of $\bar{e}_{\mathrm{r}}\left(\boldsymbol{q}_{\mathrm{M},i}\right)$ in noiseless and noisy situations before and after WC (upper:case (a), lower:case (b)).

Case (a)		
S/N (dB)	Before WC ($\times 10^{-2}\lambda$)	After WC (Proposed) ($\times 10^{-2}\lambda$)
∞	4.43	2.32
20	3.37	2.10
Case (b)		
S/N (dB)	Before WC ($\times 10^{-2}\lambda$)	After WC (Proposed) ($\times 10^{-2}\lambda$)
∞	5.33	2.64
20	4.32	2.16

receiving the reflection echo from the internal target. Also, Table 1 shows a comparison of the root-mean-square (RMS) error $e_{\mathrm{r}}\left(\boldsymbol{q}_{\mathrm{M},i}\right)$ as $\bar{e}_{\mathrm{r}}\left(\boldsymbol{q}_{\mathrm{M},i}\right)$ before and after WC in both cases. This table shows that the proposed method significantly enhances the accuracy for internal imaging by compensating the waveform deformation. Furthermore, we should mention that if the size of internal target is near to that of the dielectric medium, it is naturally difficult to estimate the relative permittivity because we cannot obtain the precise level of the transmission signal due to shadowing from the internal target with the observation model assumed in this paper.

6. Conclusion

This paper proposed a novel permittivity estimation method for a dielectric medium with an arbitrarily shaped and clear boundary, where the dielectric boundary points and their normal vectors obtained by RPM are effectively used for propagation path estimation. Moreover, to enhance the accuracy of permittivity estimation, an iterative waveform compensation scheme employing the FDTD method was incorporated, where an initial guess of the relative permittivity and dielectric boundary was employed for data regeneration. This method has a significant advantage for the conventional techniques and that it is applicable to an arbitrary and unknown dielectric boundary shape, and it thus has a non-parametric property for permittivity estimation and internal imaging. In numerical simulation based on the FDTD method, it was confirmed that our method reduced the relative errors in relative permittivity estimation to less than 6% even for S/N = 20 dB for two types of dielectric medium. As a result, the internal image obtained employing the existing technique described in [5] offers a target boundary with accuracy on the order of 1/100 of a wavelength. In our future work, we will enhance the accuracy of permittivity estimation, exploiting the information obtained using the estimated internal target.

Acknowledgment

This work is supported by the Research Grant (Basic Research) promoted by TEPCO Memorial Foundation, the Research Grant for Young Scientist promoted by the Nakajima Foundation, the Kurata Grants promoted by the Kurata Memorial Hitachi Science and Technology Foundation and the Research Grant promoted by the Tateishi Science and Technology Foundation.

References

[1] R.J. Fontana, "Recent system applications of short-pulse ultra-wideband (UWB) technology," IEEE Trans. Microw. Theory Tech., vol.52, no.9, pp.2087–2103, Sept. 2004.
[2] A. Boryssenko, O. Boryssenko, A. Lishchenko, and V. Prokhorenko, "Inspection of internal structure of walls by subsurface radar," IEEE Aerosp. Electron. Syst. Mag., vol.21, no.10, pp.28–31, Oct. 2006.
[3] X. Li, E.J. Bond, B.D. Van Veen, and S.C. Hagness, "An overview of ultra-wideband microwave imaging via space-time beamforming for early-stage breast-cancer detection," IEEE Antennas Propag. Mag., vol.47, no.2, pp.19–34, Feb. 2005.
[4] P. Kosmas and C.M. Rappaport, "A matched-filter FDTD-based time reversal approach for microwave breast cancer detection," IEEE Trans. Antennas Propag., vol.54, no.4, pp.1257–1264, April 2006.
[5] K. Akune, S. Kidera, and T. Kirimoto, "Accurate and nonparametric imaging algorithm for targets buried in dielectric medium for UWB radars," IEICE Trans. Electron., vol.E95-C, no.8, pp.1389–1398, Aug. 2012.
[6] S. Kidera, T. Sakamoto, and T. Sato, "Accurate UWB radar three-dimensional imaging algorithm for a complex boundary without range point connections," IEEE Trans. Geosci. Remote Sens., vol.48, no.7, pp.1993–2004, April 2010.
[7] A. Franchois and C. Pichot, "Microwave imaging-complex permittivity reconstruction with a levenberg-marquardt method," IEEE Trans. Antennas Propag., vol.45, no.2, pp.203–215, Feb. 1997.
[8] R. Autieri, M. Urso, T. Isernia, and V. Pascazio, "Inverse profiling via an effective linearized scattering model and MRF regularization," IEEE Geosci. Remote Sens. Lett., vol.8, no.6, pp.1021–1025, Nov. 2011.
[9] J. Ren, Y. Zhang, T. Jiang, and W. Chen, "Estimation of wall parameters from time-delay-only through-wall radar measurements," IEEE Trans. Antennas Propag., vol.59, no.11, pp.4268–4278, Nov. 2011.
[10] R. Solimene, R.D. Napoli, F. Soldovieri, and R. Pierri, "TWI for an unknown symmetric lossless wall," IEEE Trans. Geosci. Remote Sens., vol.49, no.8, pp.2876–2886, Aug. 2011.
[11] M. Dehmollaian, "Through-wall shape reconstruction and wall parameters estimation using differential evolution," IEEE Geosci. Remote Sens. Lett., vol.8, no.2, pp.201–205, March 2011.
[12] S. Kidera, T. Sakamoto, and T. Sato, "A robust and fast imaging algorithm with an envelope of circles for UWB pulse radars," IEICE Trans. Commun., vol.E90-B, no.7, pp.1801–1809, July 2007.
[13] Y. Niwa, S. Kidera, and T. Kirimoto, "Image expansion approach for target buried in dielectric medium with extended RPM to multi-static UWB radar," IEICE Trans. Electron., vol.E96-C, no.1, pp.119–123, Jan. 2013.

Ryunosuke Souma received his B.E. degrees in Electronic Engineering from University of Electro-Communications in 2011. He is currently studying for an M.M. degree at the Graduate School of Informatics and Engineering, University of Electro-Communications. His current research interest is advanced radar signal processing for UWB radar systems.

Shouhei Kidera received his B.E. degree in Electrical and Electronic Engineering from Kyoto University in 2003 and M.I. and Ph.D. degrees in Informatics from Kyoto University in 2005 and 2007, respectively. He is an assistant professor in Graduate School of Informatics and Engineering, University of Electro-Communications, Japan. His current research interest is in advanced signal processing for the near field radar, UWB radar. He is a member of the Institute of Electrical and Electronics Engineering (IEEE) and the Institute of Electrical Engineering of Japan (IEEJ).

Tetsuo Kirimoto received the B.S. and M.S. and Ph.D. degrees in Communication Engineering from Osaka University in 1976, 1978 and 1995, respectively. During 1978–2003 he stayed in Mitsubishi Electric Corp. to study radar signal processing. From 1982 to 1983, he stayed as a visiting scientist at the Remote Sensing Laboratory of the University of Kansas. From 2003 to 2007, he joined the University of Kitakyushu as a Professor. Since 2007, he has been with the University of Electro-Communications, where he is a Professor at the Graduate School of Informatics and Engineering. His current study interests include digital signal processing and its application to various sensor systems. Prof. Kirimoto is a senior member of IEEE and a member of SICE (The Society of Instrument and Control Engineers) of Japan.